Characterization of the Backbone and Side Chain Dynamics of the CaM−CaMKIp Complex Reveals Microscopic Contributions to Protein Conformational Entropy†

Kendra King Frederick, James K. Kranz,‡ and A. Joshua Wand*

Johnson Research Foundation and Department of Biochemistry and Biophysics, University of Pennsylvania, Philadelphia, Pennsylvania 19104-6059

Received May 2, 2006; Revised Manuscript Received June 19, 2006

ABSTRACT: Calmodulin is a central mediator of calcium-dependent signal transduction pathways and regulates the activity of a large number of diverse targets. Calcium-dependent interactions of calmodulin with regulated proteins are of generally high affinity but of quite variable thermodynamic origins. Here we investigate the influence of the binding of the calmodulin-binding domain of calmodulin kinase I on the fast internal dynamics of calcium-saturated calmodulin. NMR relaxation was used to probe motion on the backbone (viewed through the backbone amide NH group) and the side chains (viewed through methyl groups). The distribution of the amplitudes of side chain dynamics is trimodal. The microscopic details of side chain motion are compared with those of a thermodynamically and structurally similar complex of calmodulin with the calmodulin-binding domain of the smooth muscle myosin light chain kinase. While there are no significant differences in backbone dynamics and no net change in methyl-bearing side chain dynamics, a large redistribution of the amplitude of methyl dynamics is observed between the two complexes. The variation in dynamics was largely localized to the heterogeneously dynamic target-binding interface, suggesting that differential dynamics of the binding surface plays a functional role in the high-affinity binding interactions of calmodulin. These results begin to reveal a fundamental role for residual protein entropy in molecular recognition by calmodulin.

Changes in calcium concentration act as a ubiquitous intracellular signal that controls many different cellular processes such as secretion, muscle contraction, apoptosis, learning, memory, fertilization, and cell proliferation (*1*, *2*). In eukaryotes, calmodulin is a central mediator of Ca^{2+} signaling and interacts with a very large number of protein targets (*1*, *2*). Free calcium-saturated calmodulin (CaM)[1] consists of two globular domains connected by a solvent-exposed α-helix (*3*) that is flexible in solution (*4*). Calmodulin-binding domains are typically 15−25 amino acids in length and usually adopt an α-helical conformation in complex with CaM (*2*). There is little sequence identity between targets, but most contain two bulky hydrophobic groups that serve as anchor points for the interaction with CaM (*5*). The interaction between CaM and the target protein can be modeled by a peptide derived from the binding region of the intact target proteins (*6*).

With few exceptions, available structures of CaM−target complexes exhibit very similar tertiary structures, with a heavy atom rmsd of less than 2.5 Å between complexes. This is despite the fact that CaM-binding sequences are not conserved (*2*, *6*). How CaM is able to accommodate such a large variety of target sequences while maintaining consistently high affinity interactions, especially in the absence of large structural differences, is therefore puzzling.

While many CaM-binding domains have very similar (nanomolar) binding affinities, this binding energy has a wide range of thermodynamic origins (*7*). Isothermal titration calorimetry was used to demonstrate that similar free energies of binding could be driven by enthalpy with (e.g., the binding of the smMLCKp domain) or without (e.g., the binding of the cNOS domain) a large unfavorable change in entropy or driven by entropy with an unfavorable change in enthalpy (e.g., the binding of melittin) (*7*).

We have shown using NMR relaxation methods that CaM has a significant residual conformational entropy that is manifested in side chain motion occurring on the subnanosecond time scale (*8*). This residual entropy is redistributed

† Supported by NIH Grant DK 39806. K.K.F. is a NIH predoctoral trainee (GM 08275).

* To whom correspondence should be addressed: Department of Biochemistry and Biophysics, University of Pennsylvania, 905 Stellar-Chance Laboratories, 422 Curie Blvd., Philadelphia, PA 19104-6059. Telephone: (215) 573-7288. Fax: (215) 573-7290. E-mail: wand@mail.med.upenn.edu.

‡ Present address: Johnson & Johnson PRD, 665 Stockton Dr., Exton, PA 19341.

[1] Abbreviations: CaM, calcium-saturated recombinant chicken calmodulin; CaMKIp, peptide corresponding to the CaM kinase I calmodulin-binding domain with an ARRKWQKTGHAVRAIGRLSS sequence; smMLCKp, peptide corresponding to the smooth muscle myosin light chain kinase calmodulin-binding domain with a GSARRKWQKTGHAVRAIGRLS sequence; HSQC, heteronuclear single-quantum correlation spectroscopy; NMR, nuclear magnetic resonance; NOE, $\{^1H\}-^{15}N$ nuclear Overhauser effect; O_{NH}^2, Lipari−Szabo model-free squared generalized order parameter for the amide N−H bond vector; O_{axis}^2, Lipari−Szabo model-free squared generalized order parameter for the methyl group symmetry axis; T_1, longitudinal or spin−lattice relaxation time constant; T_2, transverse or spin−spin relaxation time constant; τ_m, correlation time for isotropic macromolecular tumbling; τ_e, Lipari−Szabo model-free effective correlation time for internal motion.

10.1021/bi060865a CCC: $33.50
Published on Web 07/25/2006

and reduced upon binding of the smMLCKp peptide (*8*). Using a simple interpretive model (*9*), the changes in the dynamics of methyl-bearing amino acid side chains were thought to correspond to a change in conformational entropy that was large enough to influence the overall binding affinity. This raises a fundamental question: Have proteins evolved to use conformational entropy to adjust or fine-tune the free energy of binding of ligands? If so, how is this achieved microscopically?

In this work, we have characterized the backbone and side chain dynamics of the complex between CaM and a peptide corresponding to the calmodulin-binding domain of the CaMKIp. We compare these dynamics to those of the CaM−smMLCKp complex and free CaM. We find that there are significant rearrangements of side chain order parameters with, however, no net change in average dynamics (entropy) between the two CaM complexes. The peptide-binding interface of CaM undergoes dynamic modulation which may explain, in part, how this small protein can bind tightly to such a diverse set of targets.

MATERIALS AND METHODS

Samples. Chicken calmodulin was expressed and purified as previously described (*10*). For the ^{2}H relaxation sample, *Escherichia coli* BL21(DES) cells were grown on minimal medium containing 55% D_2O and 45% H_2O containing $^{15}NH_4Cl$ and D-glucose (U-$^{13}C_6$, 99%) as the sole nitrogen and carbon sources, respectively. For the backbone and side chain assignment sample, cells were grown on 100% H_2O minimal medium containing $^{15}NH_4Cl$ and D-glucose (U-$^{13}C_6$, 99%). For the ^{15}N relaxation sample, cells were grown on 100% H_2O minimal medium containing $^{15}NH_4Cl$ and unlabeled glucose.

A peptide corresponding to the calmodulin-binding domain of the CaM kinase I enzyme (ARRKWQKTGHAVRAIGRLSS) was synthesized using solid phase methods and purified by reverse phase HPLC. Peptide purity was determined by mass spectrometry. Peptide concentration was determined spectrophotometrically using a theoretical extinction coefficient at 280 nm of 5690 cm^{-1} M^{-1}. CaM−CaMKIp complexes were formed by titration of ~1 mM peptide in 20 μL aliquots into 250 μM CaM under buffer conditions diluted 4-fold with respect to those of the intact complex (*11*). The titrated sample was lyophilized and rehydrated with the appropriate volume of a 92% H_2O/8% D_2O mixture. The CaM:CaMKIp stoichometery was 1:1.1. Final NMR sample conditions were 1 mM complex, 20 mM imidazole (pH 6.5), 100 mM KCl, 6 mM $CaCl_2$, and 0.02% NaN_3.

NMR Spectroscopy. All NMR data were collected at 35 °C on Varian Inova spectrometers operating at ^{1}H Larmor frequencies of 600 and 500 MHz. Sequential assignments of the backbone ^{1}H, $^{13}C_\alpha$, $^{13}C_\beta$, and ^{15}N resonances were obtained from gradient-enhanced CBCA(CO)NH and HNCACB spectra (*12*). ^{13}C and ^{1}H resonances of the side chain methyl groups were assigned using C(CO)NH (*13*) and three-dimensional $HCCH_3$-TOCSY (*14*) experiments. Stereospecific assignments for valine and leucine methyl groups were obtained using the trace [^{13}C]glucose labeling strategy (*15*). Methionine methyl resonances were assigned using a two-dimensional HMBC experiment (*16*). Although the ϵ carbons for Met72-ε and Met145-ε are well-resolved, their γ chemical shifts are identical. Assignments for these sites are those of Yuan et al. (*17*). NMR data were processed with Felix and assigned with Sparky (*18*).

^{15}N longitudinal (T_1) and transverse (T_2) relaxation time constants and the {^{1}H}−^{15}N nuclear Overhauser enhancement (NOE) were measured using experiments employing two-dimensional HSQC pulse sequences (*19*). Twelve time points ranging from 0.020 to 0.58 s (T_1) and from 7.8 to 124 ms (T_2) were collected, three of which were duplicate. Cross-peak intensities were used to quantify relaxation, and the uncertainties of these intensities were estimated from either duplicate measurements or the root-mean-square noise level of the spectrum base level. The relaxation parameters were measured at 11.7 and 16.4 T.

The dynamics of the side chain methyl groups in the protein complexes were investigated by measuring longitudinal ($I_zC_zD_z$) and transverse ($I_zC_zD_y$) relaxation rates of the ^{2}H nucleus in $^{13}CH_2D$ isotopomers (*20*). Contributions from relaxation mechanisms other than quadrupolar interactions were eliminated by correcting these rates for the decay of the I_zC_z coherence. A total of 11 time points (two of which were duplicate), ranging from 2.6 to 840 ms ($I_zC_zD_z$), from 0.9 to 26 ms ($I_zC_zD_y$), and from 8 to 220 ms (I_zC_z), were collected. ^{2}H relaxation experiments were carried out at 11.7 and 16.4 T.

Relaxation Data Analysis. Determination of dynamic parameters was accomplished by fitting the relaxation rates to the simple model-free spectral density function (*21*) with an in-house exhaustive grid search algorithm (*22*). The global rotational correlation time, τ_m, was first determined using ^{15}N relaxation data of well-ordered residues assuming isotropic rotational diffusion. Residues were excluded if the NOE value was less than 0.65 or the T_1T_2 product was more than one standard deviation from the mean (*23*). Subsequently, squared generalized order parameters and internal correlation times, τ_e, were fitted for all spectrally resolved residues. A chemical shift anisotropy tensor breadth of 170 ppm (*24*) and an effective N−H bond distance of 1.04 Å (*25*) were employed. Methyl squared generalized order parameters, O_{axis}^2, are reported after accounting for motion about the methyl symmetry axis, O^2/0.111. A quadrupolar coupling constant of 167 kHz was used in the calculations (*26*). The reliability of determined model-free parameters was estimated with 150 Monte Carlo simulations. The statistical significance of O_{axis}^2 parameter distributions was estimated using extensive randomization (*27*).

Distance Calculations. Distances to a molecular surface were calculated with GRASP (*28*). To determine the depth of burial, the solvent accessible protein surface was calculated by rolling a sphere with a radius of 1.4 Å over the van der Waals surface of the protein. Depth of burial was determined for individual sites by finding the shortest distance to this surface. Distances to the bound peptide were determined by calculating the molecular surface for the peptide and determining the shortest distance to that surface.

Isothermal Titration Calorimetry. The thermodynamic parameters governing the association of CaMKIp or smMLCKp with CaM were determined by isothermal titration calorimetry. Measurements were performed with a VP-ITC apparatus (Microcal) thermostatically regulated at 35 °C. Data were analyzed with Origin (version 5). CaM was dialyzed extensively against buffer containing 5 mM imi-

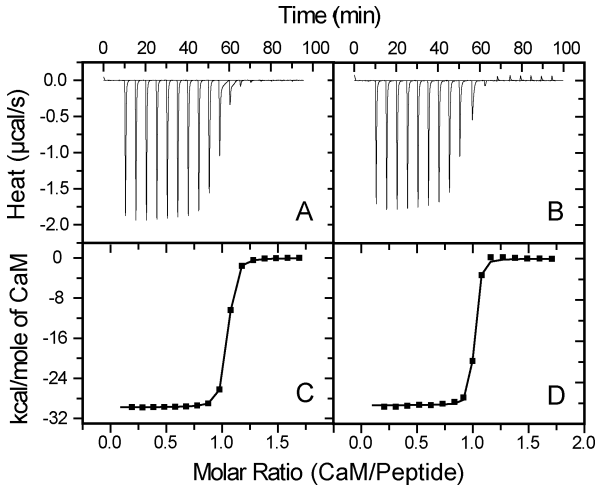

FIGURE 1: Isothermal titration calorimetry of binding of CaM to target domains. Shown are the raw heats of titration of CaM into dilute solutions of smMLCKp (A) and CaMKIp (B) peptides. The best fits of the integrated data to a single-binding site model are shown for smMLCKp (C) and CaMKIp (D). Best fit values of K_d, ΔH, and $-T\Delta S$ are given in the text. Titrations were carried out at 35 °C.

dazole, 100 mM KCl, 2 mM $CaCl_2$, and 0.02% (w/v) NaN_3 (pH 6.5). Lyophilized peptide was solubilized in the resulting dialysate and adjusted to the pH of the CaM solution with a 1 M NaOH solution made with dialysate. Concentrations of protein and peptide were determined spectrophotometrically. The peptide concentrations were 13 (CaMKIp) and 14 μM (smMLCKp) in a 1.34 mL cell volume, and 6−8 μL of 235 μM CaM was sequentially injected into the peptide solution until no further heat effects were observed. The heat of the reaction was obtained by integrating the peak after each injection of CaM using the Origin software provided with the instrument. The peaks at the end of the titration were assumed to represent the heat of dilution of CaM, which was subtracted from the data before fitting. Isotherms were analyzed using the one-site binding model provided with Origin.

RESULTS AND DISCUSSION

Isothermal Titration Calorimetry. The thermodynamic parameters underlying the formation of the CaM−CaMKIp and CaM−smMLCKp complexes were previously investigated using isothermal titration calorimetry at 25 °C and pH 7 (*7*). These experiments were essentially repeated here at pH 6.5 and 35 °C, which are more optimal for NMR spectroscopy. A typical isothermal titration calorimetry profile of the injection of CaM (235 μM) into a solution of smMLCKp or CaMKIp is shown in Figure 1. Both binding reactions are exothermic and uncomplicated and correspond to a 1:1 stoichiometry of binding. The free energy of complex formation at 35 °C for the CaM−CaMKIp complex was 49.5 ± 0.5 kJ/mol, and that for the CaM−smMLCKp complex was 46.6 ± 0.1 kJ/mol. These results mirror those obtained previously at a lower temperature and slightly higher pH (*7*).

Formation of the CaM−smMLCKp complex is slightly more enthalpically driven than formation of the CaM−CaMKIp complex. The CaM−smMLCKp complex has a favorable change in system enthalpy of −124.7 ± 0.2 kJ/mol and an unfavorable change in system entropy of 78.0 ± 0.3 kJ/mol. The change in system enthalpy for the CaM−CaMKIp complex is −119.0 ± 0.4 kJ/mol, and thus, the change in system entropy is 69.6 ± 0.9 kJ/mol. The heat of binding for targets by CaM with similar affinity can vary significantly. For example, the ΔH for binding equals −68 and 62 kJ/mol at 25 °C for smMLCKp and melittin, respectively (*7*). In this light, the thermodynamic parameters are remarkably similar for smMLCKp and CaMKIp, both of which are derived from kinase-binding domains.

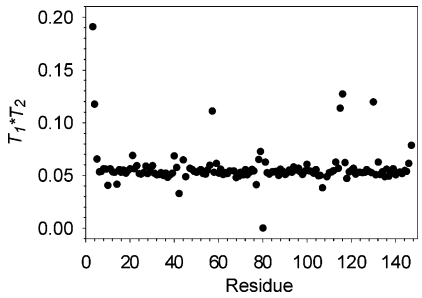

FIGURE 2: Product of T_1 and T_2 relaxation rates determined at 500 MHz (^{1}H) vs residue number. Outliers are sites that undergo chemical exchange and were fit with an additional R_{ex} term (see the text).

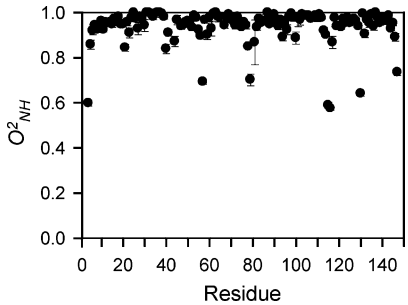

FIGURE 3: NMR-derived backbone N−H bond vector model-free squared generalized order parameters (O_{NH}^2) for CaM in complex with CaMKIp determined with relaxation data obtained at 500 and 600 MHz (^{1}H). The error bars, defined by Monte Carlo simulations, are too small to be resolved from the measured value in most cases. Non-proline residues with no entry were not determined due to spectral overlap.

Backbone Dynamics. The dynamics of main chain N−H bond vectors of calmodulin for the CaM−CaMKIp complex were measured using three ^{15}N relaxation parameters, T_1, T_2, and NOE. Using the two-parameter Lipari−Szabo formalism and an isotropic diffusion tensor, amide N−H bond vector squared generalized order parameters (O_{NH}^2) and effective internal correlation times (τ_e) were obtained for 139 of the 145 non-proline amide sites in CaM. No amide order parameters were determined for residues 1−3, the two proline residues, and residues N42, D80, D108, and K148 that had poor fits to the primary relaxation data. Fifteen sites (A10, E14, T28, L32, V35, M36, K77, E83, G98, A102, L105, R106, H107, M109, and D122) were found to have significant contributions from chemical exchange phenomena (Figure 2). These sites were fitted with an additional chemical exchange term (R_{ex}). Determined R_{ex} values ranged from 0.96 to 1.0 s^{-1}.

Amide O_{NH}^2 parameters indicate that the polypeptide backbone at this bond vector is homogeneously rigid with the exception of the linker regions and C- and N-termini (Figure 3). The distribution of backbone O_{NH}^2 parameters can be described by a Gaussian distribution ($R^2 = 0.98$)

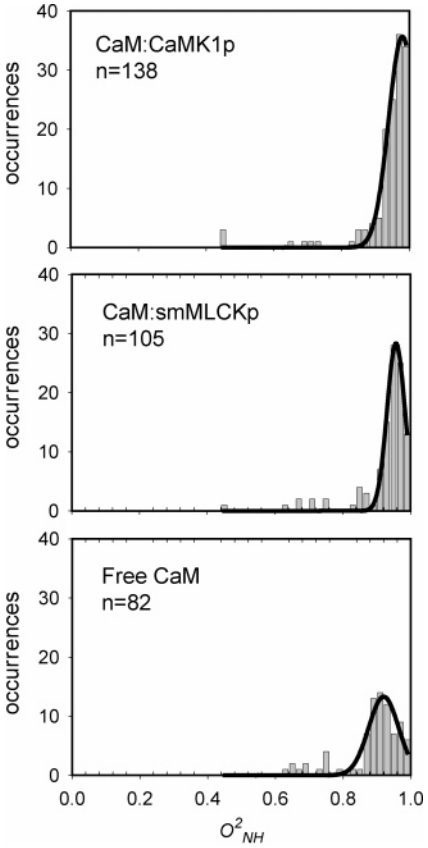

FIGURE 4: Distributions of backbone N−H bond vector model-free squared generalized order parameters (O_{NH}^2) for the CaM-CaMKIp complex, the CaM-smMLCK complex and free CaM determined with relaxation data obtained at 500 and 600 MHz (^{1}H).

centered at 0.979 ± 0.004 with a distribution width of 0.026 ± 0.002 (Figure 4). The average value for amide O_{NH}^2 parameters for free CaM is 0.891 ± 0.086 (*8*). The average difference in order parameters between free CaM and the CaM−CaMKIp complexes indicates that the backbone becomes slightly more rigid (−0.034 ± 0.017) upon formation of the complex at the 78 amides measured in both states. The formation of the CaM−CaMKIp complex results in a slight overall stiffening of the backbone.

The average difference in O_{NH}^2 values between the CaM−CaMKIp and CaM−smMLCKp complexes is, within experimental error, zero (−0.004 ± 0.018) for the 102 amides measured in both complexes (Figure 4). The largest differences in O_{NH}^2 between the two complexes occur at residues 74 and 77, where CaMKIp is more dynamic than the CaM−smMLCKp complex by ∼0.1. In the carboxy-terminal EF-hand at residues 115 and 116, the CaM−CaMKIp complex is more rigid by ∼0.1 than the CaM−smMLCKp complex. Overall, the measured amide dynamics emphasize the similarity of the response of the backbone between complexes.

Side Chain Dynamics. The amplitude of side chain motion was probed using deuterium relaxation in methyl-bearing amino acids. Side chain methyl symmetry axis squared generalized order parameters (O_{axis}^2) were determined for 66 of the 79 methyl groups in the CaM−CaMKIp complex. Relaxation data for five threonine γ2 and for Ala46 and Ala73 β-methyl groups could not be measured due to resonance overlap. Peak intensities for the Ile100-δ1, Val35-γ2, Leu112-δ1, Leu112-δ2, Leu48-δ1, and Leu69-δ2 methyls were too weak for reliable relaxation decay rates to be determined. Determined O_{axis}^2 parameters for methyl-bearing side chains range from nearly unrestrained motion (e.g., $O_{axis}^2 = 0.101$ for Met76-ε) to essentially completely restricted motion within the macromolecular frame (e.g., $O_{axis}^2 = 1.0$ for Ala88-β). As observed for large (>10 kDa) globular proteins, like flavodoxin (*29*), there is a weak correlation in the CaM−CaMKIp complex between the depth of burial of a methyl group and its O_{axis}^2 value. However, there are many exposed methyl groups that have highly restrained motions (e.g., Ala103-β $O_{axis}^2 = 0.824$) and many buried methyl groups that are highly mobile (e.g., Met51-ε $O_{axis}^2 = 0.248$ and Leu18-δ1 $O_{axis}^2 = 0.219$). Generally, depth of burial is not a good predictor of measured methyl order parameter as exemplified by Figure 5.

The O_{axis}^2 parameters in the CaM−smMLCKp complex have a striking trimodal distribution (*30*). We have termed these groupings or classes the J-, α-, and ω-classes, in accordance with the character of the motions underlying them (see below) (*31*). A similar distribution of methyl order parameters is seen in the CaM−CaMKIp complex and is fit well to a sum of three Gaussian distributions (Figure 6)

$$\text{occurrence}(O_{\text{axis}}{}^2) = \sum_{i=1}^{3} a_i \exp\left\{-\frac{1}{2}\left[\frac{O_{\text{axis}}{}^2 - \bar{O}_{\text{axis}}{}^2(i)}{\sigma_i}\right]^2\right\}$$

Fits of the histogram of the O_{axis}^2 parameters in the CaM−smMLCKp complex give distributions centered [$\bar{O}_{axis}^2(i)$] at 0.35, 0.57, and 0.79 with corresponding widths (σ_i) of 0.061, 0.068, and 0.058, respectively (Figure 6). Fits of the histogram of the O_{axis}^2 parameters in the CaM−CaMK1p complex give distributions centered [$\bar{O}_{axis}^2(i)$] at 0.40, 0.62, and 0.82 with corresponding widths (σ_i) of 0.14, 0.028, and 0.10, respectively. Extensive randomization (*27*) suggests that the obtained fitted parameters have associated p values of $<10^{-6}$ with respect to a random distribution. Though the centers of each distribution remain roughly the same in the two complexes, the widths of the J- and ω-classes are significantly larger in the CaM−CaMK1p complex. The relative population across the three classes is redistributed slightly: the α-class has a higher occupancy in the CaM−CaMK1p complex (45% vs 32%). The J- and ω-classes are both slightly lower in the CaM−CaMK1p complex (28% vs 35% and 28% vs 34%, respectively).

The bin size for this analysis was determined from a well-established formula for optimal bin width (*32*). The optimal bin width was determined independently for the J-, α-, and ω-bands on a data set that combined the observations for both of the CaM complexes. The average optimal bin width for the three classes was 0.05. Repeating this analysis for just the CaM−smMLCKp data set results in an average optimal bin width of 0.087. The result of having slightly smaller than optimal bins will result in larger errors in the Gaussian fits, whereas a larger than optimal bin size can serve to mask features of the distribution. Thus, a bin size of 0.05 was used for analysis.

Although the distinctive grouping of order parameters seen in the calmodulin complexes is often obscured in other proteins (*33*), the motional origin of these classes is clear. In the case of calmodulin, two fundamental types of motion

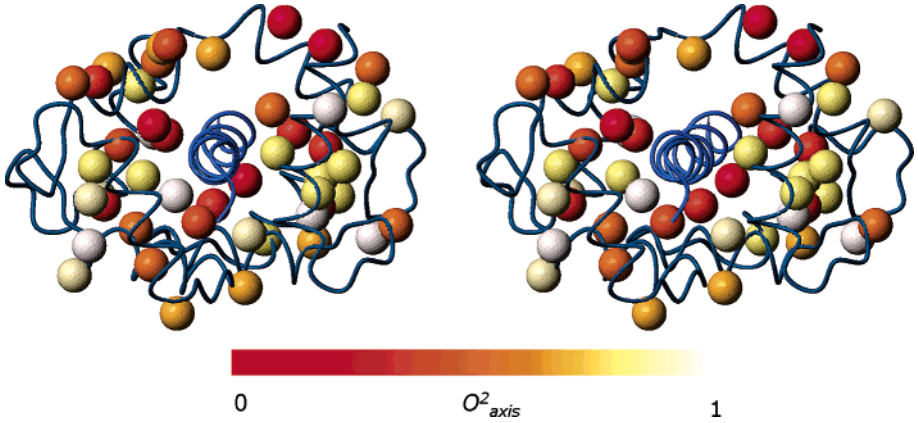

FIGURE 5: Stereoview of the distribution of methyl side chain dynamics in the CaM−CaMKIp complex. Methyl groups are represented by spheres and are color-coded with respect to the O_{axis}^2 value. This figure is based on the complex of the structure determined by Clapperton et al. [PDB entry 1MXE (*41*)]. Drawn with MolMol (*42*).

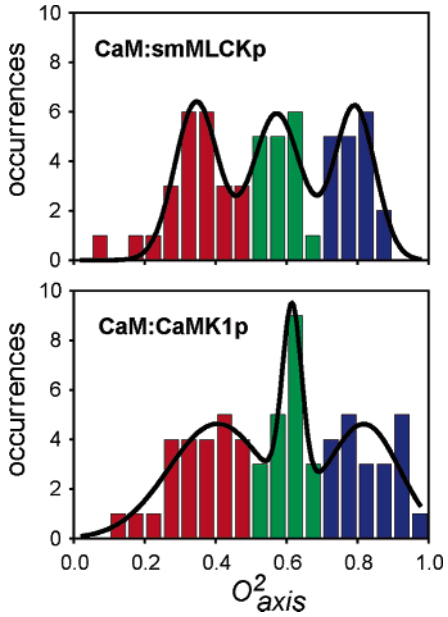

FIGURE 6: Distributions of methyl O_{axis}^2 parameters for the CaM−smMLCKp and CaM−CaMKIp complexes. Black lines represent unrestrained fits to three Gaussian distributions. Bars are colored to reflect the motional "mode" (see text). Centers for the three Gaussian distributions for CaM−smMLCKp are 0.35 ± 0.01, 0.57 ± 0.01, and 0.79 ± 0.01 (R^2 = 0.89). Centers of the Gaussian distributions for the CaM−CaMKIp complex are 0.35 ± 0.03, 0.61 ± 0.01, and 0.80 ± 0.01 (R^2 = 0.73).

occurring on the subnanosecond time scale are involved: motion within a rotamer well and motion between rotamer wells of side chain torsion angles (*34*). It has been shown that the class of motion centered on a squared generalized order parameter value of ~0.35 generally involves a contribution from rotameric interconversion on the nanosecond or faster time scale as it leads to a significant averaging of scalar coupling (*J*) constants (*34*). In the case of alanines, which cannot undergo rotomer conversion, extensive backbone motion is required. Recent experimental (*35*) and theoretical simulations (*36*, *37*) suggest this is general. The distribution of motion at the other extreme is centered on a squared generalized order parameter of ~0.8, which represents highly restricted motion within a rotamer well and is reminiscent of the relative rigidity of the polypeptide backbone. The class of motion centered on a squared generalized order parameter of ~0.6 involves little detectable rotamer interconversion and therefore reflects both variation of the amplitude of motion within a single rotamer well and the superposition of motion about connected torsion angles. The distribution within this class is generally expected to reflect the variance of the amplitude of motion within rotamer wells. We label these three groupings of side chain motion as the J-, α-, and *ω*-classes.

Of the six methyl-bearing amino acids, most contribute to all three motional classes. In the CaM−CaMKIp complex, threonines do not contribute to the J-class while alanine does not contribute to the α-class. This behavior of alanines in calmodulin is similar to the case for the CaM−smMLCKp complex and is consistent with the motional origins of the three classes. Alanine is directly connected to the main chain so all of its dynamic motions must involve motions of the polypeptide backbone. Although there are no instances of alanines participating in the intermediate α-class of motion in CaM, alanine residues with order parameters in the 0.5−0.7 range have been observed in other molecules (*31*). In contrast to those of the CaM−CaMKIp complex, threonines in the CaM−smMLCKp complex are more mobile and only contribute to the J- and α-classes of motion. Calmodulin is unusual in its high methionine content, and they are represented in all three classes of motion in both complexes.

An interesting issue is whether the dynamic response of individual side chains to the binding of different target domains is the same. There are 53 methyl sites for which O_{axis}^2 values could be reliably determined in both the CaM−smMLCKp and CaM−CaMKIp complexes. On average, the CaM−CaMKIp complex is slightly ($\langle \Delta O_{axis}^2 \rangle = -0.039 \pm 0.024$) more rigid than the CaM−smMLCKp complex. However, the average absolute difference ($\langle |\Delta O_{axis}^2| \rangle$) is 0.09, reflecting large site-to-site variability in O_{axis}^2 parameters between the two complexes (see Figure 7). Nevertheless, the O_{axis}^2 parameters of most sites stay within the same class in the CaM−CaMKIp and CaM−smMLCKp complexes. For approximately one-sixth of the sites measured, this is not the case (Figure 8). This is somewhat at odds with what is observed for comparisons between other CaM−target complexes (*38*).

Dynamic Character of the Interface. Structurally, the interface between CaM and target domains is a rich mixture of polar or ionic and hydrophobic interactions. Methionine

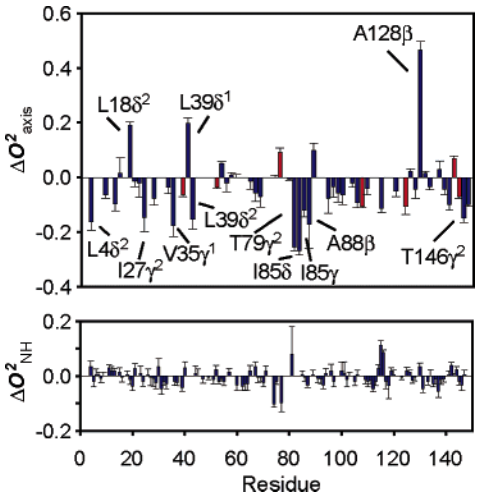

FIGURE 7: Differential response of calmodulin to the binding of the CaMKIp and smMLCKp domains. Differences (CaM−smMLCKp minus CaM−CaMKIp) in side chain methyl group O_{axis}^2 parameters (top) and backbone NH O_{NH}^2 parameters (bottom). Red bars correspond to methionine residues.

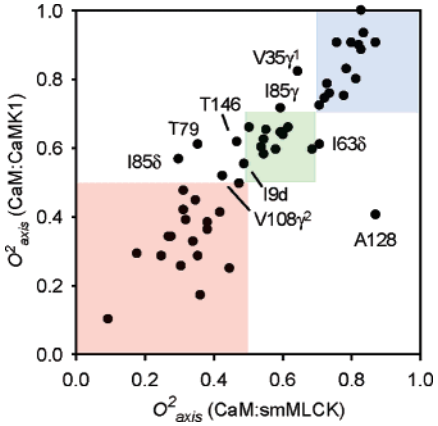

FIGURE 8: Correlation plot of methyl O_{axis}^2 parameters for the CaM−smMLCKp and CaM−CaMKIp complexes. Boxes delineate the boundaries of motional class colored as in the distribution shown in Figure 5. A number of methyl groups change their motional class between the two complexes and are labeled.

side chains dominate the hydrophobic character of the CaM-binding interface, though several other methyl-bearing amino acids also contribute to the interface between CaM and the CaMKIp domain. Methyl groups packed at the interface are

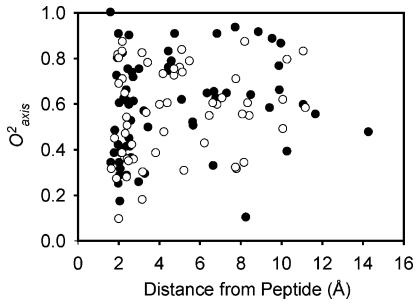

FIGURE 9: Dependence of methyl O_{axis}^2 parameters on its distance from the molecular surface of the bound target domain for the CaM−smMLCKp complex (○) and the CaM−CaMKIp complex (●).

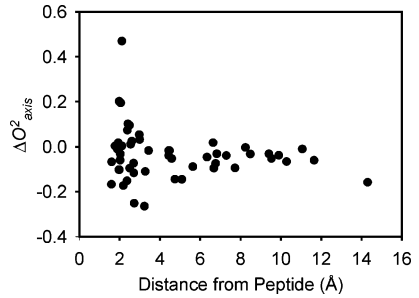

FIGURE 10: Dependence of the difference in the methyl O_{axis}^2 parameter in the CaM−smMLCKp and CaM−CaMKIp complexes on the distance from the bound target domain. Negative values correspond to sites that have larger amplitude motion in the CaM−smMLCKp complex.

heterogeneously dynamic, with O_{axis}^2 parameters ranging in value from ∼1 to 0.2 (Figure 9). Interestingly, unlike the large changes observed between the free and bound states (*8*), the differences in O_{axis}^2 parameters between the CaM−smMLCKp and CaM−CaMKIp complexes are small, with most being less than 0.2 (Figures 7 and 10). The dynamic differences between the two complexes fall off quickly as one moves from the interface (Figures 9 and 10). There is no obvious three-dimensional correlation of the differential response of the dynamics of calmodulin to the binding of the two domains (Figure 11).

Some of the more notable differences between the dynamics of the two complexes involve Ala128 and Thr79. Ala128 of CaM is much more mobile in the CaM−CaMKIp complex (0.405 ± 0.016) than it is in the CaM−smMLCKp complex

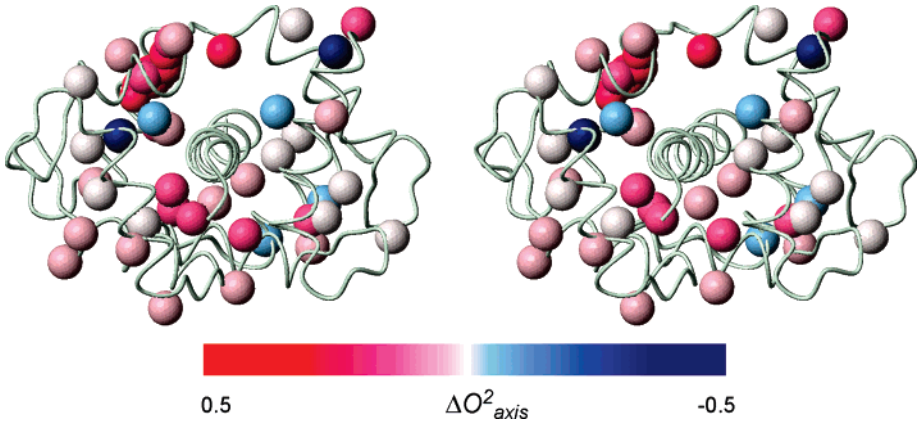

FIGURE 11: Stereoview of the distribution of differences in methyl O_{axis}^2 parameters (CaM−smMLCKp minus CaM−CaMKIp) mapped onto the crystal structure of the CaM−CaMKIp complex (PDB entry 1MXE). Red groups are more mobile in the CaM−smMLCKp complex. Drawn with MolMol (*42*).

(0.871 ± 0.027) and represents a transition from the rotamer interconverting J-class to the highly immobilized ω-class. This is particularly interesting since the backbone motion, as sensed by the amide N−H bond, is not significantly different at this site. Since the methyl of alanine is rigidly related to the backbone, this observation requires a motion that has its director aligned parallel to the amide N−H bond. Thr79 is a member of the α-class in the CaM−CaMKIp complex (0.610 ± 0.014) and moves to the rotamer interconverting J-class in the CaM−smMLCKp complex (0.355 ± 0.004). Thr79 is in the linker region between the two globular domains of free CaM. The linker takes on defined structure in both complexes. There may be an obvious structural reason for the significant difference in dynamics at this site in the two complexes. Although significantly solvent exposed in the CaM−CaMKIp complex, the hydroxyl oxygen of Thr79 is hydrogen bonded with the NH1 group of Arg16 of CaMKIp. In contrast, the side chain of Thr79 is completely solvent exposed in the CaM−smMLCKp complex.

Role of the Conformational Entropy of CaM in Target Binding. The ability of calmodulin to bind literally hundreds of target domains of quite disparate sequence but with roughly the same affinity presents a significant paradox, especially if variation of the free energy of binding is restricted to primarily structural (enthalpic) interactions. The initial observation that calmodulin undergoes a significant change in its dynamics upon binding the smMLCKp target domain raised the possibility that calmodulin employs conformational entropy to adjust target affinity (*8*). Here we have compared the CaM−CaMKIp complex to the CaM−smMLCKp complex. Thermodynamically, the binding of both the domains to CaM is enthalpically driven to almost the same degree and results in nearly identical affinities. Though the average dynamical response is similar, the microscopic origins are somewhat different, particularly at the interface between calmodulin and the bound domain.

Amino acid side chain dynamics reflect an underlying presence of residual conformational entropy (*9*, *39*, *40*). Changes in dynamics due to binding therefore illuminate contributions of residual conformational entropy of the protein to the total change in system entropy due to binding. The change in methyl-bearing amino acid side chain dynamics mirrors that of the entropy of binding. Model-dependent interpretation suggests that the contribution of the protein to the binding entropy is significant (*8*, *34*). These two results strongly support the notion that changes in the residual entropy of proteins can be used to adjust the free energy of protein−protein associations. The fact that there is not a consistent distribution of dynamics (manifesting residual entropy) in the two complexes implies that the two complexes have evolved independent solutions for modulating the entropic component contributing to the binding affinity. This reinforces a simple thermodynamic particle view of the role of the protein in setting the free energy of binding (*38*).

ACKNOWLEDGMENT

We thank Professor Mark Greene for use of the isothermal titration calorimeter and Dr. Kathy Valentine for help with the NMR relaxation experiments.

REFERENCES

1. Chin, D., and Means, A. R. (2000) Calmodulin: A prototypical calcium sensor, *Trends Cell Biol. 10*, 322−328.
2. Crivici, A., and Ikura, M. (1995) Molecular and structural basis of target recognition by calmodulin, *Annu. Rev. Biophys. Biomol. Struct. 24*, 85−116.
3. Babu, Y. S., Bugg, C. E., and Cook, W. J. (1988) Structure of calmodulin refined at 2.2 Å resolution, *J. Mol. Biol. 204*, 191−204.
4. Barbato, G., Ikura, M., Kay, L. E., Pastor, R. W., and Bax, A. (1992) Backbone dynamics of calmodulin studied by ^{15}N relaxation using inverse detected two-dimensional NMR spectroscopy: The central helix is flexible, *Biochemistry 31*, 5269−5278.
5. Rhoads, A. R., and Friedberg, F. (1997) Sequence motifs for calmodulin recognition, *FASEB J. 11*, 331−340.
6. Kranz, J. K., Lee, E. K., Nairn, A. C., and Wand, A. J. (2002) A direct test of the reductionist approach to structural studies of calmodulin activity: Relevance of peptide models of target proteins, *J. Biol. Chem. 277*, 16351−16354.
7. Brokx, R. D., Lopez, M. M., Vogel, H. J., and Makhatadze, G. I. (2001) Energetics of target peptide binding by calmodulin reveals different modes of binding, *J. Biol. Chem. 276*, 14083−14091.
8. Lee, A. L., Kinnear, S. A., and Wand, A. J. (2000) Redistribution and loss of side chain entropy upon formation of a calmodulin-peptide complex, *Nat. Struct. Biol. 7*, 72−77.
9. Li, Z., Raychaudhuri, S., and Wand, A. J. (1996) Insights into the local residual entropy of proteins provided by NMR relaxation, *Protein Sci. 5*, 2647−2650.
10. Urbauer, J. L., Short, J. H., Dow, L. K., and Wand, A. J. (1995) Structural analysis of a novel interaction by calmodulin: High-affinity binding of a peptide in the absence of calcium, *Biochemistry 34*, 8099−8109.
11. Seeholzer, S. H., and Wand, A. J. (1989) Structural characterization of the interactions between calmodulin and skeletal muscle myosin light chain kinase: Effect of peptide (576−594)G binding on the Ca^{2+}-binding domains, *Biochemistry 28*, 4011−4020.
12. Muhandiram, D. R., and Kay, L. E. (1994) Gradient-enhanced triple-resonance three-dimensional NMR experiments with improved sensitivity, *J. Magn. Reson., Ser. B 103*, 203−216.
13. Montelione, G. T., Lyons, B. A., Emerson, S. D., and Tashiro, M. (1992) An Efficient Triple Resonance Experiment Using C-13 Isotropic Mixing for Determining Sequence-Specific Resonance Assignments of Isotopically-Enriched Proteins, *J. Am. Chem. Soc. 114*, 10974−10975.
14. Uhrin, D., Uhrinova, S., Leadbeater, C., Nairn, J., Price, N. C., and Barlow, P. N. (2000) 3D HCCH3-TOCSY for resonance assignment of methyl-containing side chains in C-13-labeled proteins, *J. Magn. Reson. 142*, 288−293.
15. Neri, D., Szyperski, T., Otting, G., Senn, H., and Wuthrich, K. (1989) Stereospecific nuclear magnetic resonance assignments of the methyl groups of valine and leucine in the DNA-binding domain of the 434 repressor by biosynthetically directed fractional ^{13}C labeling, *Biochemistry 28*, 7510−7516.
16. Bax, A., Delaglio, F., Grzesiek, S., and Vuister, G. W. (1994) Resonance Assignment of Methionine Methyl-Groups and χ_3 Angular Information from Long-Range Proton-Carbon and Carbon−Carbon J-Correlation in a Calmodulin Peptide Complex, *J. Biomol. NMR 4*, 787−797.
17. Yuan, T., Gomes, A. V., Barnes, J. A., Hunter, H. N., and Vogel, H. J. (2004) Spectroscopic characterization of the calmodulin-binding and autoinhibitory domains of calcium/calmodulin-dependent protein kinase I, *Arch. Biochem. Biophys. 421*, 192−206.
18. Goddard, T., and Kneller, D. (2004) *SPARKY 3*, University of California, San Francisco.
19. Farrow, N. A., Muhandiram, R., Singer, A. U., Pascal, S. M., Kay, C. M., Gish, G., Shoelson, S. E., Pawson, T., Forman-Kay, J. D., and Kay, L. E. (1994) Backbone dynamics of a free and phosphopeptide-complexed Src homology 2 domain studied by ^{15}N NMR relaxation, *Biochemistry 33*, 5984−6003.
20. Muhandiram, D. R., Yamazaki, T., Sykes, B. D., and Kay, L. E. (1995) Measurement of ^{2}H T_1 and $T_{1\rho}$ Relaxation Times in Uniformly ^{13}C-Labeled and Fractionally ^{2}H-Labeled Proteins in Solution, *J. Am. Chem. Soc. 117*, 11536−11544.
21. Lipari, G., and Szabo, A. (1982) Model-free approach to the interpretation of nuclear magnetic resonance relaxation in macromolecules. 1. Theory and range of validity, *J. Am. Chem. Soc. 104*, 4546−4559.

22. Dellwo, M. J., and Wand, A. J. (1989) Model-Independent and Model-Dependent Analysis of the Global and Internal Dynamics of Cyclosporine-A, *J. Am. Chem. Soc. 111*, 4571−4578.
23. Kneller, J. M., Lu, M., and Bracken, C. (2002) An effective method for the discrimination of motional anisotropy and chemical exchange, *J. Am. Chem. Soc. 124*, 1852−1853.
24. Lee, A. L., and Wand, A. J. (1999) Assessing potential bias in the determination of rotational correlation times of proteins by NMR relaxation, *J. Biomol. NMR 13*, 101−112.
25. Ottiger, M., and Bax, A. (1998) Determination of relative N−H−N, N−C′, Cα−C′, and Cα−Hα effective bond lengths in a protein by NMR in a dilute liquid crystalline phase, *J. Am. Chem. Soc. 120*, 12334−12341.
26. Mittermaier, A., and Kay, L. E. (1999) Measurement of methyl H-2 quadrupolar couplings in oriented proteins. How uniform is the quadrupolar coupling constant? *J. Am. Chem. Soc. 121*, 10608−10613.
27. Edgington, E. (1995) *Randomization Tests*, 3rd ed., Marcel Dekker, New York.
28. Nicholls, A., Sharp, K. A., and Honig, B. (1991) Protein folding and association: Insights from the interfacial and thermodynamic properties of hydrocarbons, *Proteins 11*, 281−296.
29. Liu, W., Flynn, P. F., Fuentes, E. J., Kranz, J. K., McCormick, M., and Wand, A. J. (2001) Main chain and side chain dynamics of oxidized flavodoxin from *Cyanobacterium anabaena*, *Biochemistry 40*, 14744−14753.
30. Lee, A. L., and Wand, A. J. (2001) Microscopic origins of entropy, heat capacity and the glass transition in proteins, *Nature 411*, 501−504.
31. Igumenova, T. I., Frederick, K. K., and Wand, A. J. (2006) Characterization of the Fast Dynamics of Protein Amino Acid Side Chains Using NMR Relaxation in Solution, *Chem. Rev. 106*, 1672−1699.
32. Scott, D. (1979) On optimal and data-based histograms, *Biometrika 10*, 605−610.
33. Best, R. B., Clarke, J., and Karplus, M. (2004) The origin of protein sidechain order parameter distributions, *J. Am. Chem. Soc. 126*, 7734−7735.
34. Lee, A. L., Sharp, K. A., Kranz, J. K., Song, X. J., and Wand, A. J. (2002) Temperature dependence of the internal dynamics of a calmodulin-peptide complex, *Biochemistry 41*, 13814−13825.
35. Chou, J. J., Case, D. A., and Bax, A. (2003) Insights into the mobility of methyl-bearing side chains in proteins from $^{3}J_{CC}$ and $^{3}J_{CN}$ couplings, *J. Am. Chem. Soc. 125*, 8959−8966.
36. Best, R. B., Clarke, J., and Karplus, M. (2005) What contributions to protein side-chain dynamics are probed by NMR experiments? A molecular dynamics simulation analysis, *J. Mol. Biol. 349*, 185−203.
37. Hu, H., Hermans, J., and Lee, A. L. (2005) Relating side-chain mobility in proteins to rotameric transitions: Insights from molecular dynamics simulations and NMR, *J. Biomol. NMR 32*, 151−162.
38. Marlow, M. S., and Wand, A. J. (2006) Conformational dynamics of calmodulin in complex with the calmodulin dependent kinase kinase calmodulin-binding domain, *Biochemistry 45*, 8732−8741.
39. Yang, D. W., and Kay, L. E. (1996) Contributions to conformational entropy arising from bond vector fluctuations measured from NMR-derived order parameters: Application to protein folding, *J. Mol. Biol. 263*, 369−382.
40. Akke, M., Bruschweiler, R., and Palmer, A. G. (1993) NMR Order Parameters and Free-Energy: An Analytical Approach and Its Application to Cooperative Ca^{2+} Binding by Calbindin-D(9k), *J. Am. Chem. Soc. 115*, 9832−9833.
41. Clapperton, J. A., Martin, S. R., Smerdon, S. J., Gamblin, S. J., and Bayley, P. M. (2002) Structure of the complex of calmodulin with the target sequence of calmodulin-dependent protein kinase I: Studies of the kinase activation mechanism, *Biochemistry 41*, 14669−14679.
42. Koradi, R., Billeter, M., and Wuthrich, K. (1996) MOLMOL: A program for display and analysis of macromolecular structures, *J. Mol. Graphics 14*, 51−55.

BI060865A